

Engineering the spectra of photon triplets generated from micro/nanofiber

Chuan Qu(瞿川), Dongqin Guo(郭东琴), Xiaoxiao Li(李笑笑), Zhenqi Liu(刘振旗), Yi Zhao(赵义), Shenghai Zhang(张胜海), and Zhengtong Wei(卫正统)

Citation: Chin. Phys. B, 2024, 33 (**3**): 034208. DOI: 10.1088/1674-1056/ad1c5d
Journal homepage: http://cpb.iphy.ac.cn; http://iopscience.iop.org/cpb

What follows is a list of articles you may be interested in

Optimal and robust control of population transfer in asymmetric quantum-dot molecules

Yu Guo(郭裕), Songshan Ma(马松山), and Chuan-Cun Shu(束传存)
Chin. Phys. B, 2024, 33 (**2**): 024203. DOI: 10.1088/1674-1056/ad0627

Calibration and cancellation of microwave crosstalk in superconducting circuits

Haisheng Yan(严海生), Shoukuan Zhao(赵寿宽), Zhongcheng Xiang(相忠诚), Ziting Wang(王子婷), Zhaohua Yang(杨钊华), Kai Xu(许凯), Ye Tian(田野), Haifeng Yu(于海峰), Dongning Zheng(郑东宁), Heng Fan(范桁), and Shiping Zhao(赵士平)
Chin. Phys. B, 2023, 32 (**9**): 094203. DOI: 10.1088/1674-1056/acdc10

Generation of spectrally uncorrelated biphotons via fiber nonlinear quantum interference

Zhengtong Wei(卫正统), Chuan Qu(瞿川), Tian'an Wu(吴天安), Yuanyuan Li(李媛媛), Bo Li(李博), and Shenghai Zhang(张胜海)
Chin. Phys. B, 2023, 32 (**6**): 064202. DOI: 10.1088/1674-1056/acb767

Enhanced phase sensitive amplification towards improving noise immunity

Hui Guo(郭辉), Zhi Li(李治), Hengxin Sun(孙恒信), Kui Liu(刘奎), and Jiangrui Gao(郜江瑞)
Chin. Phys. B, 2023, 32 (**5**): 054204. DOI: 10.1088/1674-1056/acbdeb

Effective dynamics and quantum state engineering by periodic kicks

Zhi-Cheng Shi(施志成), Zhen Chen(陈阵), Jian-Hui Wang(王建辉), Yan Xia(夏岩), and X X Yi(衣学喜)
Chin. Phys. B, 2023, 32 (**4**): 044210. DOI: 10.1088/1674-1056/ac7bfc

---

Engineering the spectra of photon triplets generated from micro/nanofiber

Chuan Qu(瞿川), Dongqin Guo(郭东琴), Xiaoxiao Li(李笑笑), Zhenqi Liu(刘振旗), Yi Zhao(赵义), Shenghai Zhang(张胜海), and Zhengtong Wei(卫正统)†

The College of Basic Department, Information Engineering University, Zhengzhou 450000, *China*

(Received 23 November 2023; revised manuscript received 8 January 2024; accepted manuscript online 9 January 2024)

Quantum light sources are the core resources for photonics-based quantum information processing. We investigate the spectral engineering of photon triplets generated by third-order spontaneous parametric down-conversion in micro/nanofiber. The phase mismatching at one–third pump frequency gives rise to non-degenerate photon triplets, the joint spectral intensity of which has an elliptical locus with a fixed eccentricity of $\sqrt{6}/3$. Therefore, we propose a frequency-division scheme to separate non-degenerate photon triplets into three channels with high heralding efficiency for the first time. Choosing an appropriate pump wavelength can compensate for the fabrication errors of micro/nanofiber and also generate narrowband, non-degenerate photon triplet sources with a high signal-to-noise ratio. Furthermore, the long-period micro/nanofiber grating introduces a new controllable degree of freedom to tailor phase matching, resulting from the periodic oscillation of dispersion. In this scheme, the wavelength of photon triplets can be flexibly tuned using quasi-phase matching. We study the generation of photon triplets from this novel perspective of spectrum engineering, and we believe that this work will accelerate the practical implementation of photon triplets in quantum information processing.

Keywords: photon triplets, micro/nanofiber, spectrum engineering

PACS: 42.50.Dv, 42.50.Ex, 42.65.Lm, 42.81.–i **DOI:** 10.1088/1674-1056/ad1c5d

1. Introduction

Photons are well suited for the implementation of major quantum information processing (QIP) tasks, such as quantum computation,[1,2] quantum teleportation,[3] quantum key distribution,[4] and quantum metrology.[5] These photonics-based QIP creates demands for sources of single photons[6,7] and of multiple photons[5,8] in quantum-entangled states. Indeed, over the past few decades, spontaneous parametric down-conversion (SPDC) in second-order nonlinear crystals, as well as spontaneous four-wave mixing (SFWM) in third-order nonlinear fibers, have emerged as the primary choices for entangled photon pair sources in many QIP experiments.[9,10] Importantly, photon triplet states have inherent advantages in generating Greenberger–Horne–Zeilinger (GHZ) states[11] and the heralded generation of photon pairs.[12] Several methods have been reported for generating photon triplets, including cascaded photon pair processes[13] and quantum-dot molecule schemes.[14] Nevertheless, these methods are plagued by extremely low collection efficiencies. Third-order spontaneous parametric down-conversion (TOSPDC), the inverse process to third-harmonic generation (THG), where a pump photon is annihilated to simultaneously give birth to a photon triplet governed by energy and momentum conservation, may lead to the generation of GHZ states without post-selection.[15–17] Further, TOSPDC introduces three-mode squeezing operators to directly facilitate the realization of non-Gaussian states,[18,19] while two-mode squeezing operators lead to Gaussian squeezed states. Despite TOSPDC's promising prospects for QIP, it confronts some technological challenges due to the weak third-order nonlinearity of typical optical materials and difficulties in achieving phase matching.[20]

A micro/nanofiber is an optical fiber with a core diameter approaching the submicron scale, a size comparable to the wavelength of the transmitted light. Here, the effective nonlinear-optical coefficients are significantly enhanced due to the reduced mode area and field enhancement that results from tight confinement.[21,22] The typical method for fabricating micro/nanofiber involves heating and stretching standard optical fibers until they reach a predetermined diameter.[23] In addition, the use of direct mode cutoff feedback can significantly enhance the accuracy and precision of real-time diameter control during the fiber-pulling process.[23,24] Note that the cladding of the original fiber acts as the core confining light, while the surrounding air serves as the new cladding. It is such a large step in the refractive index that tightly confines the mode inside the core. Furthermore, phase matching is actually dependent on the chromatic dispersion of the fiber. The ability of a micro/nanofiber to support multiple transmission modes enables phase matching of TOSPDC through so-called intermodal phase matching, where the pump operates in a high-order mode while the photon triplets are in the fundamental mode. Also, waveguide dispersion contributes greatly to chromatic dispersion, suggesting that photon-triplet wavelengths can be widely tailored by changing the micro/nanofiber diameter. The pigtail of the micro/nanofiber is retained as a stan-

†Corresponding author. E-mail: weizhengtong1987@126.com

© 2024 Chinese Physical Society and IOP Publishing Ltd

dard optical fiber, which is beneficial for accessing the fiber quantum network with minimal coupling loss.

In this work, we study the spectrum engineering of photon triplets generated from micro/nanofibers and long-period micro/nanofiber gratings. A multitude of theoretical and experimental studies have focused on realizing phase matching for degenerate signal frequencies to improve the efficiency of photon triplet generation, using methods such as fiber dispersion tuning,[25,26] nonlinear phase modulation enhancing[27] and quasi phase matching (QPM).[28–30] Some studies have validated these design schemes experimentally through THG.[17,20] Nonetheless, spectrum engineering, especially for non-degenerate photon triplets, has rarely been reported. In fact, phase mismatching at one-third pump frequency gives rise to non-degenerate photon triplets without a decrease in efficiency. An increased phase mismatching corresponds to a broader signal bandwidth, indicating that the collection efficiency of photon triplets decreases and the noise increases. Further, the photon triplets need to be separated into three channels for practical applications in QIP. To the best of our knowledge, we provide a frequency-division scheme with high heralding efficiency for the first time. Moreover, we propose a QPM scheme to generate tunable-wavelength photon triplets in a long-period micro/nanofiber grating. The results presented can also be extended to many optical materials and waveguide geometries where TOSPDC occurs.

This paper is organized as follows. In Section 2, we introduce the quantum theory analysis of TOSPDC and give the expression of joint spectral amplitude. In Section 3, we investigate the ellipse locus of joint spectra, and based on this, in Section 4, we propose a frequency-division scheme to separate non-degenerate photon triplets into three channels. Also, we study the tunable-wavelength photon triplets based on QPM in Section 5. Conclusions and some perspectives are drawn in Section 6.

2. Photon triplet states

The TOSPDC process is a third-order optical nonlinear process, originating from the third-order susceptibility $\chi^{(3)}$. The annihilation of individual photons from the pump modes gives birth to photon triplets, as shown in Fig. 1. The three emitted signal modes are referred to as signal-1 (r), signal-2 (s), and idler (i) with angular frequencies ω_r, ω_s and ω_i, respectively. Pump angular frequency is denoted as ω_p. This TOSPDC process occurs by satisfying the energy conservation $\omega_\mathrm{r}+\omega_\mathrm{s}+\omega_\mathrm{i}=\omega_\mathrm{p}$ and phase-matching condition $\Delta\beta=\beta_\mathrm{p}-\beta_\mathrm{r}-\beta_\mathrm{s}-\beta_\mathrm{i}-\beta_\mathrm{NL}=0$, where β_j ($j=$ p, r, s, i) is the mode propagation constant for the four participating fields and β_NL is the nonlinear contribution resulting from cross and self-phase modulation.[22] $\Delta\beta$ is known as the phase mismatch.

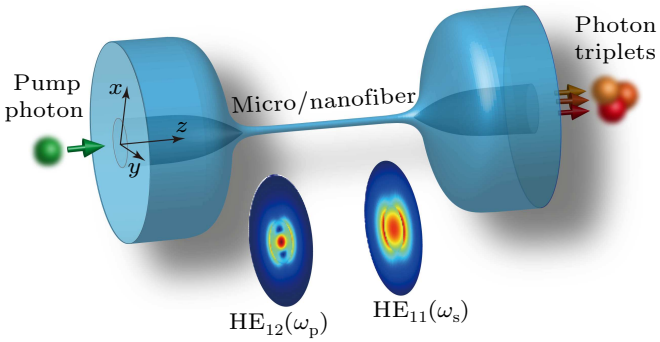


Fig. 1. The TOSPDC process in micro/nanofiber. A pump photon decays into photon triplets. Additionally, the intensity distributions of the two mode fields are shown below.

The light–matter interaction Hamiltonian for the TOSPDC is given by[20,31]

$$\hat{H}_\mathrm{I}(t) = \frac{3}{4}\epsilon_0\chi^{(3)}\int_{V_\mathrm{int}} \mathrm{d}V \hat{E}_\mathrm{p}^{(+)}(\boldsymbol{r},t)\hat{E}_\mathrm{r}^{(-)}(\boldsymbol{r},t)\hat{E}_\mathrm{s}^{(-)}(\boldsymbol{r},t)\hat{E}_\mathrm{i}^{(-)}(\boldsymbol{r},t), \quad (1)$$

where $\chi^{(3)}$ is the cubic susceptibility, ϵ_0 is the vacuum permittivity and the integral is evaluated over the cubic interaction volume V_int. The subscript i denotes the idler, and the other i signifies the imaginary unit. We describe classically the strong pump fields, in terms of monochromatic pump, its positive-frequency components can be written as

$$E_\mathrm{p}^{(+)}(\boldsymbol{r},t) = \mathcal{E}_\mathrm{p}A_\mathrm{p}(x,y)\,\mathrm{e}^{\mathrm{i}\left(\int_0^z \beta_\mathrm{p}(z')\,\mathrm{d}z'-\omega_\mathrm{p}t\right)}, \quad (2)$$

where $A_\mathrm{p}(x,y)$ represents the normalized transverse field distribution, β_p is the pump propagation constant varying along fiber length (z-axis). $\mathcal{E}_\mathrm{p}$ denotes the pump-field amplitudes, $\mathcal{E}_\mathrm{p}=\sqrt{(2P_\mathrm{p})/(\epsilon_0 cn(\omega_\mathrm{p}))}$ with pump power P_p, speed of light in vacuum c, refractive index n and pump angular frequency ω_p. Further, the weak emitted modes are described by negative-frequency components of the electric field operator $\hat{E}_\mu^{(-)}$ (with $\mu=$ r, s, i)

$$\hat{E}_\mu^{(-)}(\boldsymbol{r},t) = -\mathrm{i}\sum_{\omega_\mu}\mathcal{E}_\mu^* A_\mu^*(x,y)\hat{a}^\dagger(\omega_\mu)\,\mathrm{e}^{-\mathrm{i}\left(\int_0^z \beta_\mu(z')\,\mathrm{d}z'-\omega_\mu t\right)}, \quad (3)$$

where $A_\mu(x,y)$ represents the normalized transverse field distribution, β_μ is the mode propagation constant and $\hat{a}^\dagger(\omega_\mu)$ is the frequency-dependent creation operator. $\mathcal{E}_\mu$ denotes the field amplitudes, $\mathcal{E}_\mu=\sqrt{(2\hbar\omega_\mu)/(\epsilon_0 cn(\omega_\mu)T_\mathrm{q})}$ with reduced Planck constant $\hbar$ and quantization time T_q. The time-evolution operator is $\hat{U}_\mathrm{I}=\exp\left(\frac{1}{\mathrm{i}\hbar}\int_{-\infty}^{\infty}\mathrm{d}t\hat{H}_\mathrm{I}\right)$, in which the time integration $\int_{-\infty}^{\infty}\mathrm{e}^{-\mathrm{i}(\omega_\mathrm{p}-\omega_\mathrm{r}-\omega_\mathrm{s}-\omega_\mathrm{i})t}\,\mathrm{d}t = 2\pi\delta(\omega_\mathrm{p}-\omega_\mathrm{r}-\omega_\mathrm{s}-\omega_\mathrm{i})$ emphasizes the energy conservation rule. Using the first-order perturbation theory, the output states can be written as

$$|\psi\rangle = \left[1-\frac{\mathrm{i}}{\hbar}\int_{-\infty}^{\infty}\mathrm{d}t\hat{H}_\mathrm{I}(t)\right]|0\rangle = |0\rangle_\mathrm{r}|0\rangle_\mathrm{s}|0\rangle_\mathrm{i}+|\psi_3\rangle. \quad (4)$$

Therefore, we obtain the photon triplet states in terms of the fiber length L

$$|\psi_3\rangle = \frac{3\pi\epsilon_0\chi^{(3)}}{2\hbar}\sum_{\omega_r}\sum_{\omega_s}\sum_{\omega_i}\mathcal{E}_p\mathcal{E}_r^*\mathcal{E}_s^*\mathcal{E}_i^* f_{prsi} \times \int_0^L e^{i\int_0^z \Delta\beta(z')\,dz'}\,dz\hat{a}^\dagger(\omega_r)\hat{a}^\dagger(\omega_s)\hat{a}^\dagger(\omega_i)|0\rangle_r|0\rangle_s|0\rangle_i, \tag{5}$$

where f_{prsi} accounts for the effective interaction area among the four fields, expressed as $f_{prsi} = \iint_{int} A_p A_r^* A_s^* A_i^*\,dxdy$.

Importantly, the rates of photon-triplet emission are in direct proportion to N_r with

$$N_r = \sum_{\omega_r}\langle\psi_3|\hat{a}^\dagger(\omega_r)\hat{a}(\omega_r)|\psi_3\rangle = \frac{72\hbar P_p}{\pi}\iiint \gamma_I^2\frac{\omega_r\omega_s\omega_i}{\omega_p^2}|\mathcal{F}(\omega_r,\omega_s,\omega_i)|^2\,d\omega_r\,d\omega_s\,d\omega_i, \tag{6}$$

where γ_I is the nonlinear coefficient of the TOSPDC process, expressed as

$$\gamma_I = \frac{3\chi^{(3)}\omega_p f_{prsi}}{4\epsilon_0 c^2\sqrt{n(\omega_p)n(\omega_r)n(\omega_s)n(\omega_i)}}, \tag{7}$$

and joint spectral intensity (JSI) $|\mathcal{F}(\omega_r,\omega_s,\omega_i)|^2$ is related to the probability of photon triplets emitted at frequencies of ω_r, ω_s, and ω_i. In Eq. (6), the product term $\gamma_I^2\omega_r\omega_s\omega_i/\omega_p^2$ has a slowly-varying dependence on frequency within the spectral range of interest,[15] such that we neglect this dependence and characterize the spectral properties of photon triplets with the joint spectral amplitude (JSA) $\mathcal{F}(\omega_r,\omega_s,\omega_i)$, given by

$$\mathcal{F}(\omega_r,\omega_s,\omega_i) = \int_0^L e^{i\int_0^z\Delta\beta(z')\,dz'}\,dz. \tag{8}$$

Obviously, due to the energy conservation rule $\omega_p = \omega_r + \omega_s + \omega_i$, it can be shown that

$$\mathcal{F}(\omega_r,\omega_s,\omega_i) = \mathcal{F}(\omega_p - \omega_s - \omega_i,\omega_s,\omega_i),$$

indicating that therein lies only two free frequencies. Note that in terms of homogeneous fiber with unchanged phase mismatch $\Delta\beta(z)$ along fiber z axis, $\mathcal{F}(\omega_r,\omega_s,\omega_i)$ can be reduced as

$$\mathcal{F}(\omega_r,\omega_s,\omega_i) = Le^{i\frac{\Delta\beta L}{2}}\,\mathrm{sinc}\left(\frac{\Delta\beta L}{2}\right). \tag{9}$$

In this case, the JSI $|\mathcal{F}(\omega_r,\omega_s,\omega_i)|^2 = L^2\mathrm{sinc}^2(\Delta\beta L/2)$ and thus phase matching $\Delta\beta = 0$ corresponds to the most efficient photon-triplet emission.

Generally, the fulfillment of phase matching resorts to the so-called intra-modal phase matching, in which the pump is in a higher-order mode while the triplet photons are all in the fundamental mode (HE_{11} mode). Here, the micro/nanofiber used to generate photon triplets has a submicron diameter, such that changing diameter drastically influences the contribution of waveguide dispersion to fiber dispersion. Figure 2(a) shows the effective refractive index of various modes versus the micro/nanofiber diameter. Here, the black curve denotes the fundamental mode with a wavelength of 1551 nm (angle frequency ω_1), while the colorful curves represent higher-order modes with a wavelength of 517 nm (angle frequency ω_3, $\omega_3 = 3\omega_1$). In the case of continuous-wave (CW) pump with low peak power, the nonlinear phase mismatch β_{NL} is negligible and the phase matching is rewritten as $n_{eff}(\omega_3) = n_{eff}(\omega_1)$ corresponding to the intersections between black curve and colorful curves. Even if multiple higher-order modes enable one to fulfill the phase matching of the TOSPDC process, most of them are inaccessible due to their poor overlap integrals f_{prsi} and the difficulty in coupling pump into higher-order modes. The favorable regime occurs when the visible pump light is guided in the HE_{12} mode, and the micro/nanofiber diameter is 767 nm, corresponding to the black dot in Fig. 2(a). The pump wavelength of $\lambda_{p0} = 517$ nm and the diameter of $d_0 = 767$ nm are referred to as reference values. Moreover, the intensity distributions of the $HE_{11}(\omega_1)$ mode and the $HE_{12}(\omega_3)$ mode are shown in Figs. 2(b) and 2(c), respectively. It turns out that the overlap integral for the combination of $HE_{11}(\omega_1)$ and $HE_{12}(\omega_3)$ is the most efficient for generating photon triplets.[20]

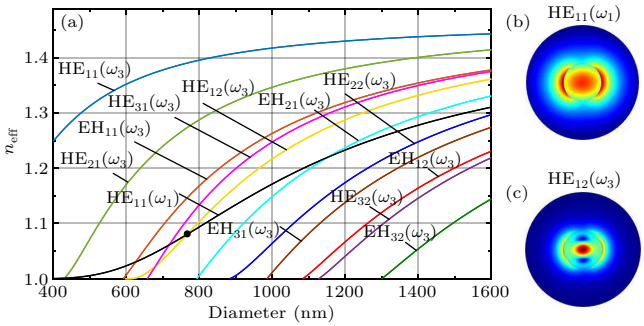


Fig. 2. (a) The dependence of the effective refractive index n_{eff} on the micro/nanofiber diameter for various higher-order modes at a wavelength of 517 nm and for the fundamental mode at a wavelength of 1551 nm. (b) and (c) The intensity distributions in terms of $HE_{11}(\omega_1)$ mode and $HE_{12}(\omega_3)$ mode, respectively.

3. Joint spectra with ellipse locus

In the process of TOSPDC, the pump wavelength and micro/nanofiber diameter may deviate slightly from their reference values, whereas the rules of energy conservation and phase matching can still be satisfied resulting from non-degenerate photon-triplet frequencies. In addition, non-degenerate TOSPDC with phase matching also maintains efficient photon-triplet emission, unlike the process of THG. Figure 3 shows the results of simulated photon-triplet JSI in the space of $\{\omega_s,\omega_i,\omega_r\}$ with brighter one representing higher probabilities of emission. As for the monochromatic pump,

the JSI is pasted upon the plane of $\omega_s+\omega_i+\omega_r=\omega_p$ due to energy conservation. Thus, we project JSI onto the three coordinate planes to obtain each marginal distribution. Here, the pump wavelength is shifted by -0.2 nm with $\lambda_p=516.8$ nm. Obviously, the non-degenerate JSI has a form of closed-loop belt and is absent from an emission maximum at the loop center with frequency of $\omega_p/3$.

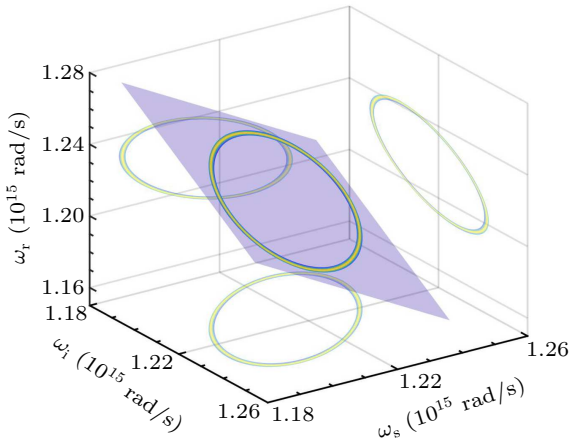


Fig. 3. JSI in the three-dimensional space of $\{\omega_s,\omega_i,\omega_r\}$ in terms of the frequency non-degenerate configuration. The violet plane stands for the plane of $\omega_s+\omega_i+\omega_r=\omega_p$. Three marginal distributions are projected on the corresponding coordinate planes.

Energy conservation enables one to fix ω_r by $\omega_r=\omega_p-\omega_s-\omega_i$, resulting in existing only two free frequencies in JSI, such that two-dimensional marginal distribution will be enough to account for photon-triplet spectral characteristics. Figures 4(a) and 4(c) show the photon-triplet JSI in the $\{\omega_s,\omega_i\}$ plane for non-degenerate regime ($\lambda_p=516.8$ nm) and degenerate regime ($\lambda_p=517$ nm). In order to analytically investigate the locus of JSI, we expand the HE_{11} mode propagation constant β_μ (with $\mu=r,s,i$) in a second-order Taylor series about the frequency $\omega_p/3$, i.e., $\beta_\mu(\omega_\mu)\approx\beta_s(\omega_p/3)+\beta_s^{(1)}(\omega_\mu-\omega_p/3)+(1/2)\beta_s^{(2)}(\omega_\mu-\omega_p/3)^2$, where $\beta_s^{(m)}=(\mathrm{d}^m\beta_s/\mathrm{d}\omega^m)_{\omega=\omega_p/3}$ with $m=1,2$. Substituting the above expansions into the phase-matching relation $\Delta\beta=0$ and using the energy conservation to simplify the linear terms, we get an ellipse locus for the frequency combinations of perfect phase matching, expressed as

$$\left(\delta_+-\frac{2\omega_p}{3}\right)^2+\frac{\delta_-^2}{3}=\frac{4\left[\beta_p-3\beta_s\left(\omega_p/3\right)+\beta_{NL}\right]}{3\beta_s^{(2)}},\quad(10)$$

where $\delta_+=\omega_s+\omega_i$ and $\delta_-=\omega_s-\omega_i$. Then, we ignore the effect of nonlinear phase matching, such that the minor semi-axis length of the ellipse can be written as $R=\sqrt{4\left[\beta_p-3\beta_s\left(\omega_p/3\right)\right]/(3\beta_s^{(2)})}$.

In the case of non-degenerate frequency, $R>0$ gives rise to an ellipse-belt JSI in shape, while in the case of degenerate frequency, $R=0$ gives rise to an ellipse-cake JSI in shape. The highest emission probabilities occur at frequencies satisfying the ellipse equation in Eq. (10) and they get identical probabilities for both of degenerate and non-degenerate cases above. Furthermore, degenerate photon triplets get a Gaussian-approximation output spectrum, while non-degenerate photon triplets get a concave output spectrum, as shown in Figs. 4(b) and 4(d). The two highest values of the concave spectrum correspond to the left/right extreme points of ellipse; using analytic geometry methods, the bandwidth of the concave spectrum reads $2\sqrt{2}R$. Note that there are multiple weak ellipse belts, attributing to the assistant peaks in sinc function plots, thus they rapidly oscillate and decay.

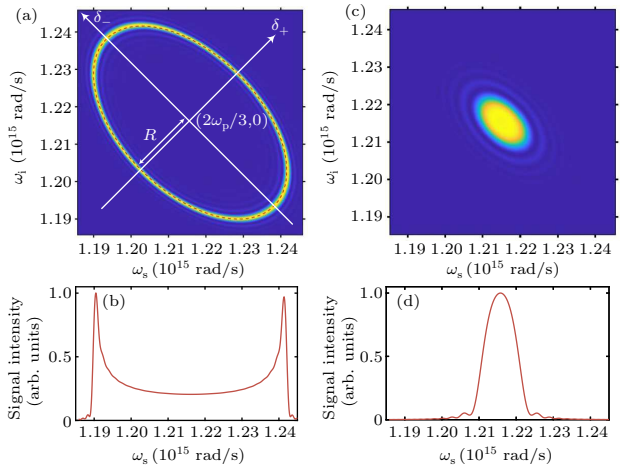


Fig. 4. JSIs in the $\{\omega_s,\omega_i\}$ plane, corresponding to the marginal distribution, for the non-degenerate regime (a) and degenerate regime (c). Both JSIs are normalized by the total conversion probability. Additionally, their normalized output signal spectra are shown in panels (b) and (d), respectively. In panel (a), the red dashed curve, originating from Eq. (10), outlines an ellipse locus representing the highest emission probability. Two white arrows denote the major axis δ_- and minor axis δ_+, and they have 135° and 45° in intersection angle with the ω_s axis, respectively. The location of the ellipse center is $(2\omega_p/3,0)$ in $\{\delta_+,\delta_-\}$ coordinate plane.

4. Frequency-division scheme to separate photon triplets into three channels

A critical procedure for a TOSPDC photon-triplet source to be practically applied to quantum information technology is to separate photon triplets into three frequency channels. Hence, detecting one of the photon triplets heralds the remaining photon pairs. Fortunately, in terms of non-degenerate photon triplets, the fixed eccentricity $\sqrt{6}/3$ in the ellipse locus of JSI provides an option of the frequency-division scheme with high-enough heralding efficiency. The frequency-division scheme we give is shown in Fig. 5, wherein the simulation parameters of JSI are identical to that in Fig. 4(a). Here, the diagonal line in equation of $\omega_s=\omega_i$ intersects the ellipse of perfect phase matching at two points, accordingly, we can divide the whole spectrum into three channels.

We assume an ideal rectangular filter and that channels 1, 2 and 3 are of identical bandwidth. Therefore, we can obtain visually the channels in which s-signal and i-signal photons are located from the marginal JSI in the $\{\omega_s,\omega_i\}$ plane. Identifying the channel where r-signal photons are located is crucial

for increasing efficiency. If $\omega_s+\omega_i=2\omega_p/3+\nu$ with ν representing the frequency deviation, we have $\omega_r=\omega_p/3-\nu$. For example, in terms of point A in Fig. 5, ν indicates the vertical distance from the white dashed line $\omega_s+\omega_i=2\omega_p/3$. Then we move the point $(\omega_p/3,\omega_p/3)$ with $-\nu$ to obtain the channel of r-signal photons. Particularly, the heralding efficiency in terms of Fig. 5 is up to 94.4%.

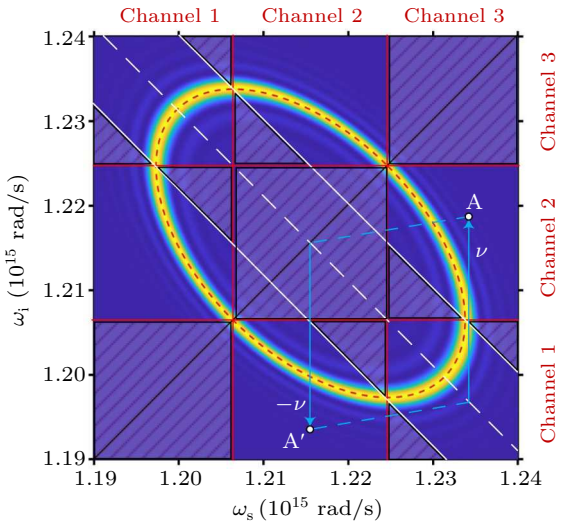


Fig. 5. Frequency-division scheme to separate non-degenerate photon triplets into three channels. The frequency-division channels 1, 2 and 3 are divided by the red lines. The coordinate equation for the white dashed line is $\omega_s+\omega_i=2\omega_p/3$ and the coordinate equations for the two solid lines are $\omega_s+\omega_i=2\omega_p/3\pm R/\sqrt{2}$. Thus, these shadow regions represent that photon triplets can not be absolutely separated, resulting in a slight decrease in heralding efficiency.

In Fig. 5, these shadow regions correspond to that photon triplets may not be absolutely separated into three channels, while other regions correspond to complete separation. Obviously, a degenerate source of photon triplets will give rise to a low heralding efficiency. In fact, the decrease in heralding efficiency mainly arises from the thickness of the ellipse belt as well as the assistant peaks of the sinc function. Both of the above-mentioned flaws can be mitigated by increasing the fiber length (see Eq. (9)). In addition, the broad ellipse loci suffer from a lot of fluorescent background, such that the frequency-division bands collecting signal photons should be set narrow enough to increase the signal-to-noise ratio.

The frequency-division scheme is realised using a frequency divider. The fabrication of this frequency divider can utilize the same technologies as the wavelength-division multiplexer in fiber communication systems. Furthermore, in order to increase the heralding efficiency, the frequency-channel edge should be steep and the channel position in the spectrum should align with the preset value.

Due to a fixed eccentricity of the ellipse locus, the bandwidth of photon triplets depends on the minor semi-axis length R. Figure 6 shows R^2 versus pump wavelength shifts $\lambda_p-\lambda_{p0}$ in terms of various micro/nanofiber diameter deviations $d-d_0$. The black dashed line marks $R=0$, indicating degenerate photon triplets. A positive R^2 corresponds to non-degenerate photon triplets, while a negative R^2 represents an unaccessible generation of photon triplets in the absence of phase matching. Obviously, around the reference value, the simultaneous decrease in micro/nanofiber diameter and increase in pump wavelength will result in the disappearance of photon triplets. As shown in Fig. 7, the ellipse width can be adjusted by changing the diameter and pump wavelength. Due to the square root function form of R, the ellipse loci in Figs. 7(a) and 7(b) become denser from the inside out. Furthermore, changing the pump wavelength will move the ellipse center, while changing the diameter will keep the ellipse center fixed. Importantly, even if the diameter deviation from the reference value, resulting from micro/nanofiber fabrication error, may broaden the bandwidths of the photon triplets or destroy phase matching, choosing an appropriate pump wavelength can compensate for this error and give rise to a narrowband, non-degenerate photon triplet source, as illustrated in Fig. 7(c). In addition, as can be seen from Fig. 7(a), a pump with a wider spectrum will result in broadening the thickness of the ellipse belt, thereby lowering the heralding efficiency. Therefore, it is necessary to choose pumps with narrow enough bands.

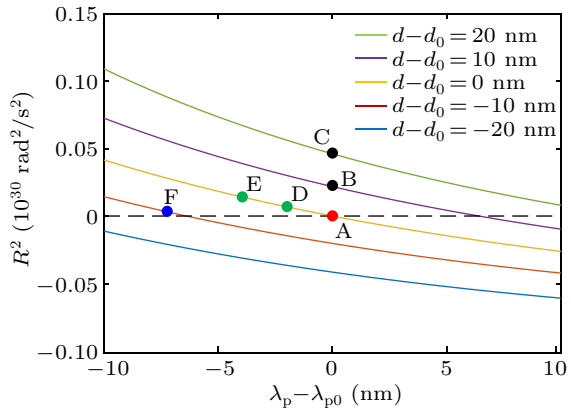


Fig. 6. The R^2 versus pump wavelength shifts $\Delta\lambda_p=\lambda_p-\lambda_{p0}$ in terms of various micro/nanofiber diameter deviations $\Delta d=d-d_0$. $\lambda_{p0}=517$ nm and $d_0=767$ nm are the reference values for pump wavelength and micro/nanofiber diameter, respectively, to perform degenerate perfect phase matching. Point A corresponds to $\Delta\lambda_p=0$ and $\Delta d=0$.

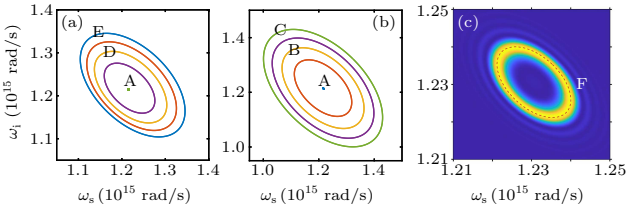


Fig. 7. (a) Ellipse loci corresponding to various $\Delta\lambda_p$ of 0 nm, −1 nm, −2 nm, −3 nm and −4 nm in the order from the inside out. (b) Ellipse loci corresponding to various Δd of 0 nm, 5 nm, 10 nm, 15 nm and 20 nm in the order from the inside out. (c) JSI with $\Delta\lambda_p=-6.42$ nm and $\Delta d=-10$ nm. Some plots marked with capitals A–F correspond to the dots in Fig. 6.

5. Tunable-wavelength photon triplet generation

Many applications of quantum information technique require multiple wavelengths, thus it is demanding to control the phase matching for adjusting the photon triplet wavelength. Phase matching mainly depends on the dispersion characteristics of fibers, whereas after finishing the fabrication of micro/nanofiber, its waveguide and material dispersion both are fixed, indicating a poor tunability of photon-triplet wavelength, as illustrated in Fig. 6. Here, long-period micro/nanofiber grating emerges as a viable candidate for realizing tunable-wavelength photon triplet source, in which the periodic variation of dispersion along fiber length provides a new controllable degree of freedom to tailor phase matching. In general, the fiber grating is modeled as adding cosine oscillation term to the original refractive index, i.e., $n(z) = n_0 + \Delta n \cos(2\pi z/\Lambda)$, where n_0 is the original refractive index, Δn denotes modulation depth of refractive index and Λ is the grating pitch.[32] Note that Δn performs differently for different fiber modes. Therefore, we rewrite the phase mismatching as

$$\Delta\beta(z) = a + b\cos\left(\frac{2\pi z}{\Lambda}\right), \tag{11}$$

where a presents the original phase mismatch without the effects of grating, while $b = \Delta n_3\omega_\mathrm{p}/c - \Delta n_1(\omega_\mathrm{s}+\omega_\mathrm{i}+\omega_\mathrm{r})/c$, reduced to $b = \omega_\mathrm{p}(\Delta n_3 - \Delta n_1)/c$ according to energy conservation. Here, Δn_3 and Δn_1 denote the modulation depth of refractive index for HE_{12} and HE_{11} modes, respectively. Further, the accumulated phase mismatch from 0 to z can be written as

$$\int_0^z \Delta\beta(z')\mathrm{d}z' = az + \frac{b\Lambda}{2\pi}\sin\left(\frac{2\pi}{\Lambda}z\right). \tag{12}$$

Substituting Eq. (12) into Eq. (8) to obtain the JSA

$$\begin{aligned}
&\mathcal{F}(\omega_\mathrm{r},\omega_\mathrm{s},\omega_\mathrm{i}) \\
&= \int_0^L \mathrm{e}^{\mathrm{i}\int_0^z \Delta\beta(z')\mathrm{d}z'}\mathrm{d}z \\
&= \sum_{q=-\infty}^{q=+\infty} J_q\left(\frac{b\Lambda}{2\pi}\right)\int_0^L \mathrm{e}^{\mathrm{i}\left(a+\frac{2\pi q}{\Lambda}\right)z}\mathrm{d}z \\
&= L\sum_{q=-\infty}^{q=+\infty} \mathrm{e}^{\mathrm{i}\left(\frac{a}{2}+\frac{\pi q}{\Lambda}\right)L} J_q\left(\frac{b\Lambda}{2\pi}\right)\mathrm{sinc}\left(\frac{a+2\pi q/\Lambda}{2}L\right),
\end{aligned} \tag{13}$$

where q stands for integer and $J_q(\cdot)$ denotes the Bessel function. The updated JSA consists of many sinc functions, independent of each other, with the maximum amplitude $J_q\left(\frac{b\Lambda}{2\pi}\right)$. So $a + 2\pi q/\Lambda = 0$ is the so-called QPM. Figure 8 shows the plots of the Bessel function for various q. Bessel functions perform decaying oscillation as x increases and have an unlimited number of extreme values and zeros. Importantly, we can adjust a by changing pump wavelength to realize QPM with respect to different q, such that the wavelength of photon triplets becomes tunable.

Figure 9 shows the JSIs of q-order QPM by using long-period micro/nanofiber gratings. The preset ones are $q = 2$ and $q = -2$, respectively. JSI shows multiple concentric ellipse loci due to QPM, and each ellipse locus corresponds to a q. From the inside out, q increases sequentially. Indeed, the minor semi-axis length of the q-order ellipse is given by

$$R_q = \sqrt{\frac{4(a+2\pi q/\Lambda)}{3\beta_\mathrm{s}^{(2)}}}. \tag{14}$$

On the one hand, as shown in Fig. 9(a), no photon triplets are generated in such a homogeneous micro/nanofiber configuration due to the absence of phase matching, while QPM enables the regeneration of photon triplets. On the other hand, as shown in Fig. 9(c), QPM can reduce the width of ellipse and thus improve the signal-to-noise ratio. Here, $q = 0$ corresponds to the homogeneous micro/nanofiber.

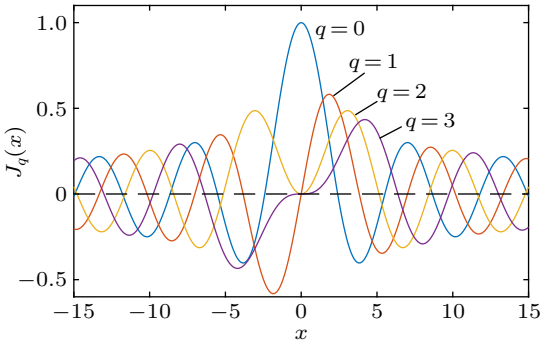


Fig. 8. The plots of Bessel function $J_q(x)$ for various q. Parity, $J_q(-x) = (-1)^q J_q(x)$.

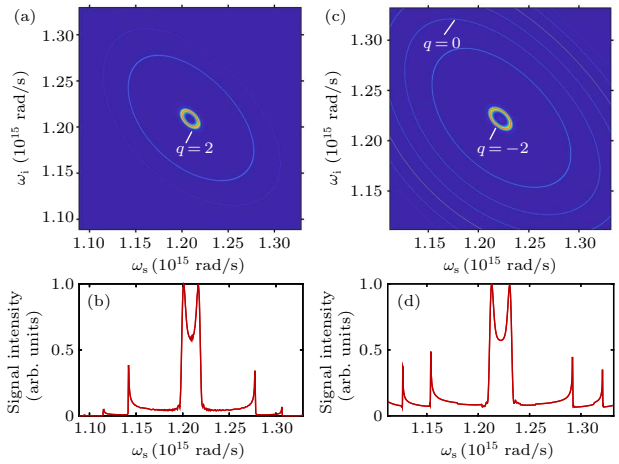


Fig. 9. (a) and (c) JSIs for the q-order QPM. Panels (b) and (d) are the normalized output signal spectra of TOSPDC corresponding to panels (a) and (c), respectively. The diameter of micro/nanofiber is the reference value 767 nm, fiber length $L = 5$ cm and grating pitch $\Lambda = 800$ μm. $\Delta n_3 - \Delta n_1 = 0.00198$ and $\lambda_\mathrm{p} = 519.75$ nm for panels (a) and (b), $\Delta n_3 - \Delta n_1 = 0.00196$ and $\lambda_\mathrm{p} = 514.24$ nm for panels (c) and (d).

To enhance the intensity of preset q-order ellipse locus and reduce the influences of other orders, the modulation depth of refractive index needs to be set at a proper value in which $b\Lambda/2\pi$ corresponds to the first extreme point of $J_q(x)$. Thus,

it is necessary to change the modulation depth of the refractive index as needed. Here, we provide a feasible suggestion that mechanically induced long-period fiber gratings, as discussed in Refs. [33,34]. Moreover, the thickness of outer ellipse belts is too thin to accumulate stronger intensity contributions. Figures 9(b) and 9(d) show that the outer ellipse loci contribute much to the overall output spectra, but these contributions are mainly concentrated outside the frequency-division band, at the same time, the central part of the spectra corresponding to the preset ellipse locus exhibits a very prominent intensity. Using the frequency-division scheme presented in Section 4, we can effectively eliminate the influences from undesired orders of QPM.

6. Conclusion

We theoretically investigate the engineering of photon-triplet spectra generated from micro/nanofiber. Firstly, we provide the expression of JSA in the process of TOSPDC. Indeed, the JSI is correlated with the probability of photon-triplet emission. The most efficient emission occurs when phase matching is fulfilled, resorting to intra-modal phase matching where the pump is in HE_{12} mode while the photon triplets are all in HE_{11} mode. Further, the two-dimensional JSI shows an ellipse locus with a fixed eccentricity of $\sqrt{6}/3$. Accordingly, we present a frequency-division scheme to separate photon triplets into three channels with high heralding efficiency. The decrease in heralding efficiency primarily results from the thickness of the ellipse belt as well as the assistant peaks of the sinc function. Both of them can be mitigated by increasing the fiber length. In particular, the width of the ellipse locus depends on the phase mismatching at one–third pump frequency, such that one can adjust the width of the ellipse locus via changing pump wavelength or micro/nanofiber diameter. Importantly, choosing an appropriate pump wavelength can compensate micro/nanofiber fabrication errors and give rise to a narrowband non-degenerate photon triplet source with a high signal-to-noise ratio. Notably, long-period micro/nanofiber gratings exhibiting periodic oscillation of dispersion along the fiber length provide a new controllable degree of freedom to tailor phase matching. Thus, QPM is introduced and plays a dominant role in the generation of tunable-wavelength photon triplets. We believe that this work provides a unique pathway towards tunable-wavelength photon triplet sources with high signal-to-noise ratios for applications in quantum information technologies.

Acknowledgments

Project supported by the National Natural Science Foundation of China (Grant No. 61605249) and the Science and Technology Key Project of Henan Province of China (Grant Nos. 182102210577 and 232102211086).

References

[1] Walmsley I A and Raymer M G 2005 *Science* **307** 1733
[2] Deng Y H, Gu Y C, Liu H L, Gong S Q, Su H, Zhang Z J, Tang H Y, Jia M H, Xu J M, Chen M C, Qin J, Peng L C, Yan J, Hu Y, Huang J, Li H, Li Y, Chen Y, Jiang X, Gan L, Yang G, You L, Li L, Zhong H S, Wang H, Liu N L, Renema J J, Lu C Y and Pan J W 2023 *Phys. Rev. Lett.* **131** 150601
[3] Valivarthi R, Puigibert M G, Zhou Q, Aguilar G H, Verma V B, Marsili F, Shaw M D, Nam S W, Oblak D and Tittel W 2016 *Nat. Photonics* **10** 676
[4] Yin H L, Chen T Y, Yu Z W, Liu H, You L, Zhou Y, Chen S, Mao Y, Huang M Q, Zhang W J, Chen H, Li M J, Nolan D, Zhou F, Jiang X, Wang Z, Zhang Q, Wang X B and Pan J W 2016 *Phys. Rev. Lett.* **117** 190501
[5] Qin J, Deng Y H, Zhong H S, Peng L C, Su H, Luo Y H, Xu J M, Wu D, Gong S Q, Liu H L, Wang H, Chen M C, Li L, Liu N L, Lu C Y and Pan J W 2023 *Phys. Rev. Lett.* **130** 070801
[6] Shukhin A A, Keloth J, Hakuta K and Kalachev A A 2020 *Phys. Rev. A* **101** 053822
[7] Kim J H, Ihn Y S, Kim Y H and Shin H 2019 *Opt. Lett.* **44** 447
[8] Fang B, Menotti M, Liscidini M, Sipe J E and Lorenz V O 2019 *Phys. Rev. Lett.* **123** 070508
[9] Anwar A, Perumangatt C, Steinlechner F, Jennewein T and Ling A 2021 *Rev. Sci. Instrum.* **92** 041101
[10] Garay-Palmett K, Kim D B, Zhang Y, Domínguez-Serna F A, OLorenz V and U′Ren A B 2023 *J. Opt. Soc. Am. B* **40** 469
[11] Niu X L, Gong Y X, Zou X B, Huang Y F and Guo G 2009 *J. Mod. Opt.* **56** 936
[12] Shalm L K, Hamel D R, Yan Z, Simon C, Resch K J and Jennewein T 2012 *Nat. Phys.* **9** 19
[13] Hübel H, Hamel D R, Fedrizzi A, Ramelow S, Resch K J and Jennewein T 2010 *Nature* **466** 601
[14] Khoshnegar M, Huber T, Predojević A, Dalacu D, Prilmüller M, Lapointe J, Wu X, Tamarat P, Lounis B, Poole P J, Weihs G and Majedi H 2017 *Nat. Commun.* **8** 15716
[15] Corona M, Garay-Palmett K and U′Ren A B 2011 *Phys. Rev. A* **84** 033823
[16] Hammer J, Cavanna A, Pennetta R, Chekhova M V, Russell P S J and Joly N Y 2018 *Opt. Lett.* **43** 2320
[17] Moebius M G, Herrera F, Griesse-Nascimento S, Reshef O, Evans C C, Guerreschi G G, Aspuru-Guzik A and Mazur E 2016 *Opt. Express* **24** 9932
[18] Zhang D, Cai Y, Zheng Z, Barral D, Zhang Y, Xiao M and Bencheikh K 2021 *Phys. Rev. A* **103** 013704
[19] González E A R, Borne A, Boulanger B, Levenson J A and Bencheikh K 2018 *Phys. Rev. Lett.* **120** 043601
[20] Cavanna A, Hammer J, Okoth C, Ortiz-Ricardo E, Cruz-Ramirez H, Garay-Palmett K, U′Ren A B, Frosz M H, Jiang X, Joly N Y and Chekhova M V 2020 *Phys. Rev. A* **101** 033840
[21] Tong L, Zi F, Guo X and Lou J 2012 *Opt. Commun.* **285** 4641
[22] Agrawal G 2013 *Nonlinear Fiber Optics* 5th edn. (Academic Press)
[23] Xu Y, Fang W and Tong L 2017 *Optics Express* **25** 10434
[24] Kang Y, Gong J, Xu Y, Yao N, Fang W, Guo X and Tong L 2020 *IEEE Photon. Technol. Lett.* **32** 219
[25] Warren-Smith S C, Chemnitz M, Schneidewind H, Kostecki R, Ebendorff-Heidepriem H, Monro T M and Schmidt M A 2017 *Opt. Lett.* **42** 1812
[26] Hao Z, Jiang B, Ma Y, Yi R, Jin H, Huang L, Gan X and Zhao J 2023 *Phys. Rev. Appl.* **19** L031002
[27] Jiang X, Zhang D, Lee T and Brambilla G 2018 *Opt. Lett.* **43** 2728
[28] Saleh M F 2018 *Phys. Rev. A* **97** 013850
[29] Jiang X, Lee T, He J, Khudus M I M A and Brambilla G 2017 *Opt. Express* **25** 22626
[30] Tarnowski K, Kibler B, Finot C and Urbanczyk W 2011 *IEEE J. Quantum Electron.* **47** 622
[31] Mandel L and Wolf E 1995 *Optical Coherence and Quantum Optics* (Cambridge: Cambridge University Press)
[32] Amiri I S, Rashed A N Z and Yupapin P P 2020 *J. Opt. Commun.* **2019** 0187
[33] Savin S V, Digonnet M J F, Kino G S and Shaw H J 2000 *Opt. Lett.* **25** 710
[34] Torres-Gómez I, Ceballos-Herrera D E and Salas-Alcantara K M 2020 *Sensors* **20** 622